JOURNAL OF GEOPHYSICAL RESEARCH: SPACE PHYSICS, VOL. 118, 7472–7481, doi:10.1002/2013JA019429, 2013

# The thresholds of ionospheric plasma instabilities pumped by high-frequency radio waves at EISCAT

C. J. Bryers,[1] M. J. Kosch,[1,2] A. Senior,[1] M. T. Rietveld,[3] and T. K. Yeoman[4]

Received 10 September 2013; revised 23 October 2013; accepted 8 November 2013; published 27 November 2013.

[1] We test the existing theories regarding the thresholds for the parametric decay instability (PDI), the oscillating two-steam instability (OTSI), and the thermal parametric instability (TPI) using the European Incoherent Scatter (EISCAT) facility's ionospheric heater. In these processes, the pump wave can couple to various electrostatic waves in the *F* layer ionosphere, which can be observed using the EISCAT UHF radar (PDI and OTSI) or by HF radar (TPI). On 19 October 2012, the heater power was stepped from ∼0.5 MW to ∼100 MW effective radiated power in seven steps using a 1 min on, 1 min off cycle. We use an electric field model, taking into account *D* region absorption, to compare theory with our observations. In all three cases, we find good agreement. In addition, the growth of striations formed during the TPI causes anomalous absorption of the heater wave, which we observe as decreased UHF ion line and plasma line backscatter power. We show evidence that heating for a prolonged period of time reduces the UHF ion line intensity throughout the experiment.

**Citation:** Bryers, C. J., M. J. Kosch, A. Senior, M. T. Rietveld, and T. K. Yeoman (2013), The thresholds of ionospheric plasma instabilities pumped by high-frequency radio waves at EISCAT, *J. Geophys. Res. Space Physics*, *118*, 7472–7481, doi:10.1002/2013JA019429.

## 1. Introduction

[2] Experiments which involve the heating of the ionosphere using powerful, high-frequency (HF) radio waves have been performed at many locations around the globe since the early 1970s. Large-scale density and temperature enhancements, artificial aurora, as well as the generation of plasma waves as a result of the HF modification have been detected using incoherent scatter radar and optical diagnostics [e.g., *Ashrafi et al.*, 2006; *Jones et al.*, 1986; *Brändström et al.*, 1999]. An *O*-mode polarized electromagnetic pump wave can couple to electrostatic plasma waves through parametric instabilities if the pump electric field exceeds certain thresholds in the region close to the reflection altitude. An *X*-mode polarized wave will reflect before it can reach the correct altitude and so cannot stimulate such instabilities, which explains why higher electron temperature enhancements are often seen when pumping with an *O*-mode wave [*Stubbe and Kopka*, 1983]. The higher temperature enhancements occur due to the low propagation velocities of the plasma waves compared to the electromagnetic wave so the energy is more efficiently absorbed by the plasma [*Robinson*, 1989]. The pump wave drives the plasma instabilities and loses energy as a result. This process is known as anomalous self-absorption.

[3] As the pump wave approaches its reflection height, the group velocity of the electromagnetic wave tends to zero, as a consequence, the electric field is enhanced and becomes orientated parallel with respect to the external magnetic field [*Rietveld et al.*, 1993]. This swelling of the electric field means that even moderate pump powers can exceed the instability thresholds. The so-called plasma instability region extends approximately 0.1 *H* km below the reflection height, where *H* is the plasma scale height given by $H = k_B(T_e + T_i)/gm_i$, where $k_B$ is the Boltzmann constant, $T_e$ and $T_i$ are the electron and ion temperatures, respectively, $g$ is the acceleration due to gravity, and $m_i$ is the ion mass. Outside of this region, the Landau damping of the electrostatic waves becomes too great to support the plasma waves [*Stubbe and Kopka*, 1981]. The purposes of this study are to test the existing theories regarding the thresholds of several instabilities and to compare them with experimental results.

[4] An incoherent scatter radar, which operates by detecting weak backscatter from longitudinal electrostatic waves, is able to detect these plasma oscillations when the Bragg backscatter condition is met; i.e., the wavelength of a plasma wave is half that of the radar. Each thermal electron in the ionosphere reradiates some of the transmitted power from the radar due to Thomson scattering. This scattering cross section is small but is enhanced when a plasma wave is present. The spatial structure of the plasma wave causes

[1]Department of Physics, Lancaster University, Lancaster, UK.
[2]School of Physics, University of KwaZulu-Natal, Durban, South Africa.
[3]EISCAT Scientific Association, Ramfjordmoen, Norway.
[4]Department of Physics and Astronomy, University of Leicester, Leicester, UK.

Corresponding author: C. J. Bryers, Department of Physics, Lancaster University, Lancaster LA1 4YB, UK. (c.bryers@lancaster.ac.uk)


2169-9380/13/10.1002/2013JA019429

Bragg scattering, and the received signal is enhanced [*Evans*, 1969]. This gives rise to the double humped ion spectra corresponding to ion acoustic waves propagating toward and away from the radar as well as the often weak upshifted and downshifted plasma lines which are signatures of Langmuir waves. Langmuir waves are fast oscillations of the electrons with the ions at rest. In an ion acoustic wave, the electrons and ions move in phase due to the electrostatic force between them. In the presence of an electromagnetic pump wave, these plasma waves can be significantly enhanced in the plasma instability region. The height at which the incoherent scatter radar detects the pump-enhanced waves is known as the matching height where the Bragg scatter condition is met.

[5] One such instability is the parametric decay instability (PDI); a three-wave interaction in which the pump wave, with angular frequency $\omega_o$, couples to two electrostatic waves ($\omega_l$ and $\omega_{ia}$) so that the following relation is satisfied [*Fejer*, 1979]:

$$\omega_o = \omega_l + \omega_{ia} \tag{1}$$

where $\omega_l$ is a high-frequency Langmuir wave and $\omega_{ia}$ is an ion acoustic wave of a much lower frequency. Langmuir waves have a frequency given by *Fejer* [1979]:

$$\omega_l \sim \omega_p \left(1 + \frac{\omega_c^2}{2\omega_p} \sin^2\theta + \frac{3}{2} k_l^2 h^2\right) \tag{2}$$

where $\omega_p$ is the plasma frequency, $\omega_c$ is the electron gyrofrequency, $\theta$ is the angle between the Langmuir wave wave number $k_l$ and the magnetic field direction, and $h^2 = \epsilon_0 k_B T_e / n_e e^2$ where $\epsilon_0$ is the permittivity of free space, $n_e$ is the electron density, and $e$ is the electron charge.

[6] A radar with the frequency $f_r$ is able to observe Langmuir and ion acoustic waves at the matching altitude $z_a$ according to *Stubbe et al.* [1992]:

$$z_a = z_0 - 12 \frac{k_B T_e f_r^2}{m_e c^2 f_0^2} H \tag{3}$$

where $z_0$ is the reflection height, $m_e$ is the electron mass, and $f_0$ is the pump wave frequency. This equation satisfies the Bragg condition in that the wavelength of the radar is twice that of the plasma wave being observed. The daughter Langmuir waves associated with the PDI can also decay further. Ion acoustic waves associated with this so-called cascade process can be observed at $z_b$ in the absence of Langmuir waves:

$$z_b = z_0 - 3 \frac{k_B T_e f_r^2}{m_e c^2 f_0^2} H \tag{4}$$

[7] If the resolution of the incoherent scatter radar is less than the difference between $z_a$ and $z_b$, which is $\sim$ 3 km, then both ion acoustic waves will be observed in the same range gate. The reason no cascade Langmuir waves are observed at $z_b$ is because the waves created here do not satisfy the matching condition of the radar.

[8] The Langmuir wave dispersion relation given by equation (2) is only weakly dependent upon the Earth's magnetic field and so it is often neglected when considering the electric field thresholds of the PDI and oscillating two-stream instability. In the derivation of these thresholds, *Fejer* [1979] assumes that the direction of the pump wave electric field is parallel to the magnetic field in the region close to reflection, which is true for high-latitude experiments. *Fejer* [1979] derived the electric field threshold for the PDI:

$$E_{\mathrm{PDI}}^2 = 4 \frac{n_e k_B T_i \nu}{\omega_p \epsilon_0 B_{\max}} \tag{5}$$

where $\nu$ is the electron collision frequency and $B_{\max}$ is a function of $T_e/T_i$. For $T_e/T_i = 2, B_{\max} = 0.56$, and for $T_e/T_i = 3, B_{\max} = 0.58$. (See Figure A1 of *Stubbe et al.* [1984] for other values of $B_{\max}$.) Once the threshold has been exceeded by a pump wave, the natural ion acoustic wave amplitudes are increased and consequently, a larger backscattered power is received by the radar.

[9] Another type of instability is the oscillating two-stream instability (OTSI) where the electromagnetic pump wave decays into two Langmuir waves and a zero-frequency, nonpropagating, spatially periodic structure [*Stubbe and Kopka*, 1981]. This means that when the OTSI is excited, a signature is seen in the radar ion line spectra at a zero-frequency offset. This is often called an enhanced central peak. The plasma line spectrum is also enhanced and is offset from the radar frequency by exactly the heater frequency. The electric field threshold for the OTSI is given by *Stubbe and Kopka* [1981]:

$$E_{\mathrm{OTSI}}^2 = 4 \frac{T_e + T_i}{T_i} \frac{n_e k_B T_i \nu}{\omega_p \epsilon_0} \tag{6}$$

since $(T_e + T_i)/T_i$ is at least equal to 2 for $T_e = T_i$, the electric field threshold for the OTSI is higher than that of the PDI.

[10] A third instability that is of interest in the current study is the thermal parametric instability (TPI). *Vaskov and Gurevich* [1975] suggested that small-scale field-aligned irregularities (striations) are generated by an *O*-mode pump wave close the upper hybrid resonance (UHR) height where the pump wave is equal to the UHR frequency, $\omega_u$:

$$\omega_o^2 = \omega_u^2 = \omega_c^2 + \omega_p^2 \tag{7}$$

[11] They show that the pump wave is scattered into electrostatic waves which propagate perpendicular to the magnetic field direction and the instability requires an initial, small density irregularity to begin. *Das and Fejer* [1979] modified the work of *Vaskov and Gurevich* [1975] to remove the need for the initial density irregularity of a certain critical amplitude as did *Grach and Trakhtengerts* [1975]. They did this by considering the nonuniform nature of the pump field. The detection of the striations is highly aspect sensitive and can only be detected when a radar beam is near orthogonal to the magnetic field. *Fialer* [1974] showed that the backscattered power reduced by 20 dB when pointing 3° away from perpendicular.

[12] The threshold electric field required to generate striations is given by *Robinson* [1989] and *Das and Fejer* [1979]:

$$E_{\mathrm{TPI}}^2 = 2.44 \frac{T_{e0}^2 \omega_o^2 k_B^2 k \cos\phi}{p \nu \omega_c e^2 H} \mathrm{e}^{-2\nu H/c} \tag{8}$$

where $T_{e0}$ is the unperturbed background electron temperature, $k$ is the striation wave number, $\phi$ is the angle between the local vertical and the magnetic field, $c$ is the speed of

light, and $p$ is the ratio of the reflected to the transmitted pump power. Initially, during the first few seconds of heating, $p$ can be approximated as 1. When the pump wave electric field exactly matches the threshold of TPI, the striation will be maintained and when it is well above the threshold, the amplitude of the striations will grow explosively. For typical $F$ region plasma parameters, the threshold for TPI is similar to that of PDI by *Robinson* [1989]. The growth time of the striations is of the order of a few seconds [*Stubbe et al.*, 1982], compared to the millisecond growth time of the PDI/OTSI [*Jones et al.*, 1986].

[13] A secondary diagnostic of the TPI and striations involves monitoring the stimulated electromagnetic emission (SEE) received on the ground. These emissions are produced by the HF pump wave at an altitude close to the reflection height. The first observation of this phenomena was made by *Thidé et al.* [1982] near Tromsø, and since then, many structures have been observed within the SEE spectra [*Leyser*, 2001]. The most common feature is the continuum which contains a peak found at the pump frequency $f_0$ with an often highly asymmetric broad upshifted and downshifted width. A second common feature is the downshifted maximum (DM) which is found in the lower sideband of the SEE spectrum. The DM is observed when upper hybrid (UH) waves, which have been excited by the pump wave, decay into a daughter UH wave and a lower hybrid (LH) wave. The daughter UH wave scatters from the striations and gives rise to the observed SEE [*Shvarts and Grach*, 1997]. The model of *Leyser et al.* [1994] accurately predicts the experimental observations of the DM absence when pumping on a gyroharmonic frequency. *Frolov* [1991] confirmed with simultaneous observations of the DM and field-aligned irregularities that the DM excitation is closely related to the formation of striations. *Leyser et al.* [1989] showed that when pumping close to the gyroharmonics, the DM does not develop. The same occurs for striation development since it is known to minimize on the gyroharmonics [*Honary et al.*, 1999].

[14] It has been shown that the structure of the DM around its peak is highly asymmetric with the highest-frequency component offset from the pump frequency being independent of the pump frequency. The frequency offset at the peak of the DM structure from the heater frequency is given by $\Delta f_{\mathrm{DM}} = 2 \times 10^{-3} f_0$ [*Stubbe et al.*, 1984]. The downshift of the highest frequency component of the DM, $\Delta f$, is given by the LH frequency, $\omega_{\mathrm{LH}} = [\omega_c \omega_i/(1 + \omega_c^2/\omega_p^2)]^{1/2}$ where $\omega_i$ is the ion gyrofrequency [*Leyser et al.*, 1990]. $\Delta f$ for the lower frequency parts of the DM, including the peak, becomes larger with increasing pump frequency, $f_0$ [*Leyser et al.*, 1994]. *Leyser et al.* [1994] found that $\Delta f_{\mathrm{DM}}$ is independent of pump power for the same frequency and has been experimentally confirmed by ourselves for the experiment reported here. They also show that by increasing pump power and decreasing it again, an hysteresis effect on the DM power occurs similar to that shown by *Wright et al.* [2006] for the Co-operative UK Twin-Located Auroral Sounding System (CUTLASS) radar backscatter power. This preconditioning effect with the pump power also affects the DM growth time, with preconditioned ionospheres showing a faster growth. Preconditioning is an effect whereby after the ionosphere has been modified by heating and not left to sufficiently cool back to its unperturbed state and striations have not decayed fully. *Bond et al.* [1997] showed that the striation decay time varied between 50–200 s depending upon the time of day, with decay times being longer toward dusk.

## 2. Modeling

[15] To study and test the validity of the theories regarding the thresholds of the PDI, OTSI, and TPI instabilities, we use an electric field model to estimate the HF wave electric field and compare the results with the data recorded during a specially designed experiment. The following sections outline the electric field model, and we present the data from two radars and SEE equipment used to detect the onset of the instabilities.

### 2.1. Electric Field Model

[16] We calculate the electric field thresholds discussed in section 1 and compare them to the electric field of the electromagnetic pump wave for different pump powers. *Löfas et al.* [2009] and *Gustavsson et al.* [2010] employed the electric field model of *Shoucri and Morales* [1984] which can be used to estimate the electric field of a pump wave at any altitude as it approaches reflection and found it to be reliable at modeling the electron temperature as measured by an incoherent scatter radar.

[17] *Shoucri and Morales* [1984] treat the electric field by two different methods depending upon the altitude. The first regime is from the lower $F$ region ~120 km to $z_m$, and the second from $z_m$ to $z_r$, where $z_r$ is the reflection height of the pump wave and $z_m$ is 300 m below $z_r$ [*Thomson*, 1970]. In this highest region, a correction due to the airy-like behavior is needed as the electric field of the pump wave begins to swell as it approaches reflection. When working in the region below $z_m$, where the radar matching height observes the plasma resonances, we do not consider the electric field in the higher regime.

[18] *Shoucri and Morales* [1984] show that the electric field $E(z)$ for an $O$-mode wave, when the altitude $z$ is below $z_m$ is given by:

$$E(z) = E(0)[\epsilon(0)/\epsilon(z)]^{1/4} \left\{ [A(0)/A(z)]^{1/2} \cdot \exp[ik_0 \int_0^z \mathcal{N}(z)\,\mathrm{d}z] + R[A(0)/A(2z_r - z)]^{1/2} \cdot \exp[-ik_0 \int_0^z \mathcal{N}(z)\,\mathrm{d}z] \right\} \tag{9}$$

where $E(0)$ is the electric field at the bottom of the $F$ region which has been reduced due to $D$ region absorption, $\epsilon(z)$ is the dielectric tensor, A(z) is the HF beam cross section at $z$, $k_0$ is the vacuum wave number, $R$ is the reflection coefficient, and $\mathcal{N}(z)$ is the complex index of refraction. Since the pump power varies within the heater beam, the electric field strength will be different at various points in space. We also model the beam refraction and use the pump power of the wave which intersects the radar beam at the matching height where the plasma waves are detected.

[19] The reflection coefficient has the following form [*Budden*, 1961]:

$$R = -i \exp\left[-2ik_0 \int_0^{z_r} \mathcal{N}(z)\,\mathrm{d}z\right] \tag{10}$$

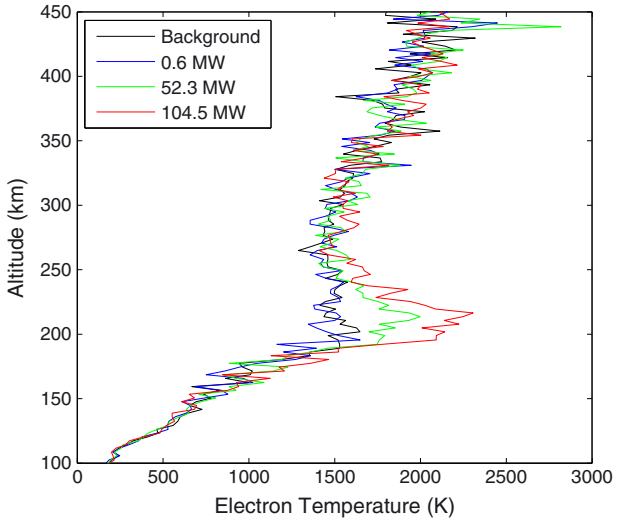


**Figure 1.** Three electron temperature profiles for various heater powers.

[20] The electric field in free space is given by:

$$E_0 = \left(\frac{\mu_0}{\epsilon_0}\right)^{0.25} \sqrt{\frac{1}{\mathcal{N}}} \sqrt{\frac{1}{4\pi}} \frac{\sqrt{\mathrm{ERP}}}{R_F} \tag{11}$$

where $\mu_0$ is the permeability of free space, effective radiated power (ERP) is the pump power on the ground, and $R_F$ is the distance to the bottom of the $F$ region.

[21] We now have a solution of the electric field of the pump wave which accounts for the swelling of the electric field as it approaches reflection which can be compared to the electric field thresholds of the instabilities.

### 2.2. *D* Region Absorption

[22] In order to account for the $D$ region absorption of the pump wave, we use the model of *Senior et al.* [2010]. We use a median background (pump off) electron density profile from 60 to 120 km taken from the UHF radar measurements. The model also considers the self-absorption of the HF wave as it causes an increase in the electron-neutral collision frequency due to the heating of the $D$ region plasma. We require the use of this model in order to reduce the free space electric field which is used in calculating equation (9).

## 3. Experiment and Data

[23] To study the onset of the three plasma instabilities, an experiment was performed on 19 October 2012 at the European Incoherent Scatter (EISCAT) Scientific Association heating facility [*Rietveld et al.*, 1993], near Tromsø, northern Norway (69.58°N, 19.21°E). The goal of the experiment was to compare the theoretical electric field thresholds of the PDI, OTSI, and TPI given by equations (5), (6), and (8), respectively, to the modeled electric field of the pump wave to test their agreement. By varying the heater power, we aimed to pump at a level well below the onset of the PDI, between PDI and OTSI, and above OTSI. We can detect which regime we are in by observing the different signatures seen in the radar data discussed in section 1.

[24] The heater was operated from 12:20 to 13:02 UT in a 1 min on, 1 min off cycle, increasing in power for each subsequent pulse. The pump polarization used was $O$-mode with a frequency of 7.953 MHz, and the seven heater effective radiated powers (ERPs) were 0.6, 2.1, 4.9, 10.5, 26.3, 52.3, and 104.5 MW for the 9°S pointing direction. Refraction meant that this wave passed through the UHF radar beam at the matching altitude. Four heater transmitters in phased array 1 were used to achieve the low powers which causes the beam width to be wider than when all 12 transmitters are in use. During the experiment, $f_o$F2 dropped from 10 MHz to 9 MHz meaning the heating was performed in an overdense ionosphere.

[25] The EISCAT facility's UHF radar [*Baron*, 1984] was measuring the plasma parameters during the experiment such as electron density and electron and ion temperatures. The UHF radar was field aligned (13°S). The radar code used enabled measurements from 50 to 700 km in altitude with a minimum of 5 s resolution and an unambiguous range resolution of 3 km. Using the data measured by the UHF incoherent scatter radar, it is possible to accurately estimate the plasma instability thresholds for the PDI and OTSI. The downshifted plasma line was also recorded by the UHF radar during the experiment.

[26] The Co-operative UK Twin-Located Auroral Sounding System (CUTLASS) HF radar at Hankasalmi, Finland (62.32°N, 26.61° E), part of the Super Dual Auroral Radar Network [*Greenwald et al.*, 1995; *Chisham et al.*, 2007], was in operation during the experiment to measure the coherent backscattered power from the pump-induced field-aligned irregularities (striations). Beam 5 was pointing over EISCAT with a range resolution of 15 km recording data with an integration time of 3 s. The CUTLASS radar was therefore used to detect the TPI by using striations as a proxy.

[27] During the experiment, SEE recording equipment was also used to measure the electromagnetic emissions from within the heated ionosphere. This was located approximately 12 km NW of EISCAT in Tromsø. The equipment composed of an active magnetic loop antenna and a digital receiver whose frequency and timing was set by GPS. The sample rate was 625 kHz, and the receiver was tuned to the pump frequency.

## 4. Results and Discussion

[28] Figure 1 shows three 60 s integrated electron temperature profiles for various pump powers. It is clear that the highest power (104.5 MW) produces a larger temperature enhancement compared to the two lower powers of 52.3 MW and 0.6 MW. The profile given in black shows the electron temperature for when the pump is off. For the lowest pump power, no enhancement is observed. This is due to low ohmic heating from the pump electromagnetic wave but primarily because weak or no resonances are stimulated to provide additional heating. *Bryers et al.* [2012] showed that for $O$-mode pumping, the energy from the pump wave is absorbed by the electrons close to the UHR height, and heat conducts up and down the magnetic field. The highest enhanced electron temperatures shown in Figure 1 are localized between 180 and 260 km. The electrons lose their energy via various cooling mechanisms and cool to background temperatures farther away from the UHR height.

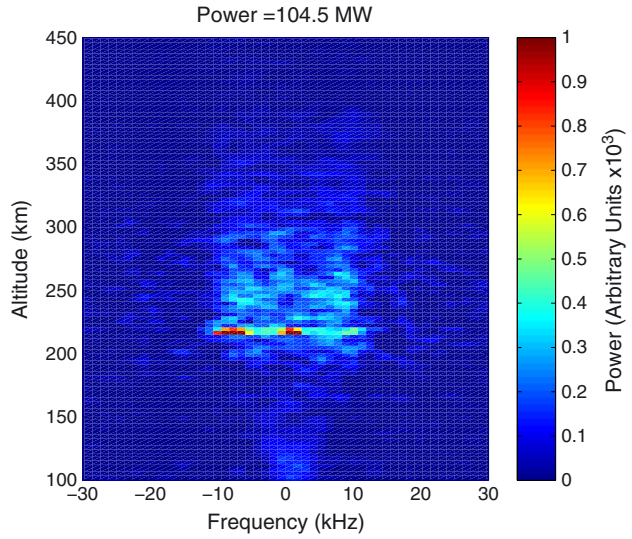


**Figure 2.** A typical UHF radar ion line spectrum. The spectrum shown is for the first 5 s during pump on with a power of 104.5 MW ERP.

[29] Figure 2 shows a typical UHF radar ion line spectrum during pumping with a high-power (104.5 MW) HF wave. In the *F* region, the usual double humped spectrum can be seen where the ion acoustic waves propagate toward and away from the radar. In the *D* region, only a single peak is observed due to the greater ion-neutral collision frequency since the neutrals are more abundant at lower altitudes. This increased collision frequency as compared the *F* region means that the ion acoustic waves cannot propagate before becoming damped. The radar therefore does not see Doppler-shifted ion lines as a result.

[30] In Figure 2, at approximately 218 km, just below the *O*-mode pump wave reflection altitude of 220 km, the enhanced ion acoustic shoulders formed during the PDI can be seen at ∼10 kHz offset above and below the radar frequency of 931 MHz. The central peak at 0 kHz offset, owing to the nonpropagating density irregularity developed during the OTSI, is also a prominent feature. In the absence of PDI and OTSI, as is the case during pump off, or when pumping with low powers below the thresholds, these features will not be present and a typical ion line profile is observed. For lower heater powers where the enhancements still exist, the profile is the same as for the 104.5 MW example shown here.

[31] During the experiment (12:20–13:02 UT), the seven pump ERP cycle of 1 min on, 1 min off ran 3 times. Figure 3 shows an overview of the UHF radar ion line spectra for every pump-on. The ion line spectra shown are for the first 5 s integration during heating. The altitude at which they are shown is where the enhancement was at a maximum (217–220 km). Where no clear enhancement is observed, the altitude selected is also within this range and is shown for comparison. For the low pump powers, the usual double humped spectra can be observed. As the pump power increases and the HF wave couples to ion acoustic and Langmuir waves, the enhancement in the shoulders is clear. This is most obvious during the first cycle for the 26.3 MW pump ERP where one shoulder is enhanced and no central peak is observed at 0 kHz offset from the radar frequency. The downshifted shoulder is preferentially enhanced indicating that the strongest ion acoustic wave is traveling away from the UHF radar. Increasing the pump power further shows that the upshifted shoulder also becomes enhanced,

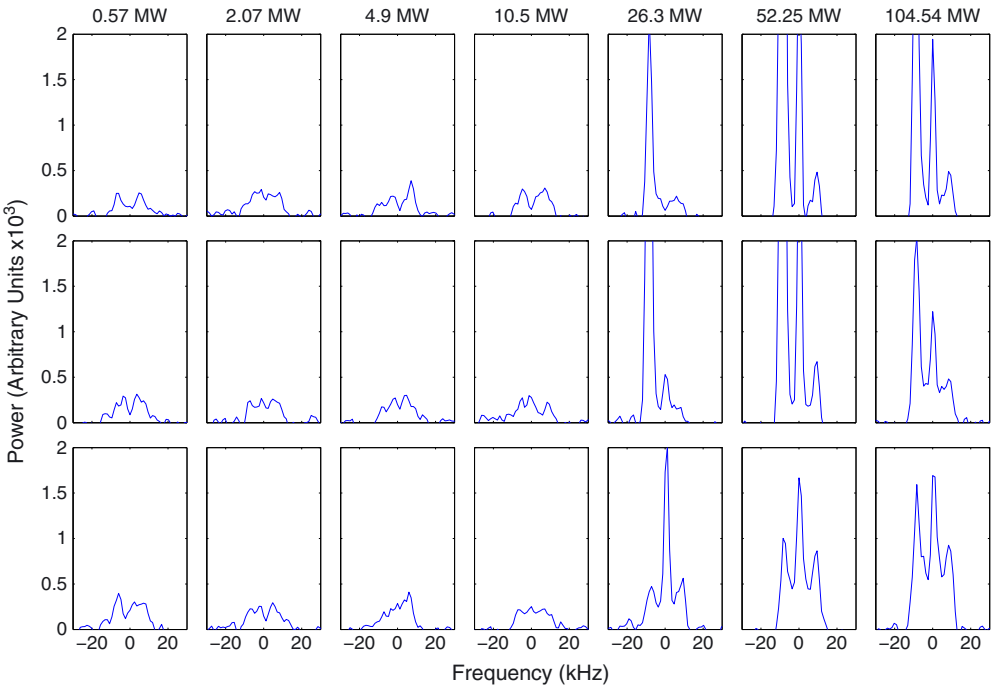


**Figure 3.** The first 5 s integration during pump on of the UHF radar ion line. The heater power was increased along each row, and the cycle was run 3 times. The altitude at which these ion lines are shown is where the enhancement was at a maximum. Where no clear enhancement is seen, the altitude shown is close to the HF reflection height.

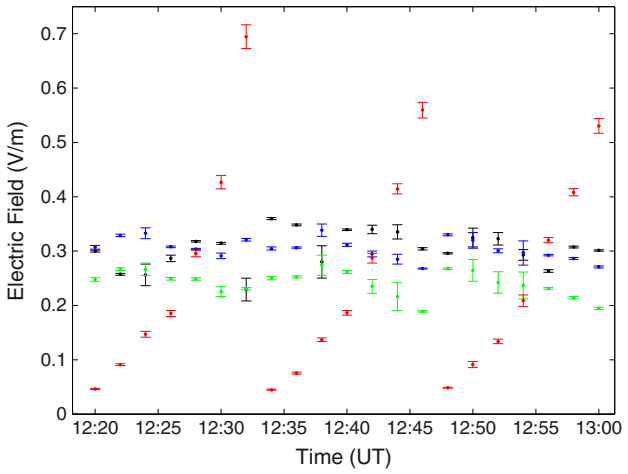


**Figure 4.** Modeling of the pump wave electric field for three cycles of the seven power steps (red). The OTSI electric field threshold (blue), the PDI threshold (green), and the TPI threshold (black).

along with an enhancement at the center frequency. An upgoing pump wave decays into a downward propagating Langmuir wave and an upward propagating ion acoustic wave [*Fejer*, 1979]. Since the pump wave is strongest in power when traveling upward, before anomalous absorption occurs, the downshifted ion line will be preferentially enhanced. Upshifted ion line shoulder enhancement can occur from the decay of the reflected pump wave or from the cascade process, where a downward propagating Langmuir wave can decay into a downward propagating ion acoustic wave.

[32] As discussed in section 1, the enhanced shoulders are an indication that the PDI has been excited since the pump wave generates ion acoustic waves, whereas the OTSI does not. The enhanced central peak, most noticeable for the highest pump powers, is a signature of the OTSI whereby a stationary density irregularity is produced. In the first of the three cycles, the PDI signature is observed in absence of the OTSI peak when the heater ERP was 26.3 MW. For the last two cycles, the power step between the heater pulses with powers 10.5 MW and 26.3 MW is too great and the PDI and OTSI appear simultaneously. Here the pump wave electric field must increase from below the threshold of PDI to above that of the OTSI within this one step and indicates that the thresholds must be relatively close to each other.

[33] Figure 4 shows the result of modeling the pump wave electric field and the three thresholds discussed in section 1. The red points show the pump wave electric field strength calculated at the matching height (∼3 km below the pump wave reflection height of ∼220 km). The blue points show the electric field threshold for the OTSI at the matching height using equation (6). The green points show the threshold for PDI calculated using equation (5), and the black dots show the threshold for TPI calculated using equation (8). In calculating the TPI threshold, the parameter $p$, which is the ratio of the reflected to the transmitted pump wave, was set to 1 since initially there are no striations and therefore anomalous absorption is low at the start of pump on. The error bars are found by calculating the thresholds and electric field of the pump wave by taking into consideration the uncertainty in the parameters measured by the UHF radar.

[34] The electric field strength of the pump wave was calculated using equation (9). The electric field at the bottom of the $F$ region (120 km) was calculated using equation (11) and was reduced due to $D$ region absorption. The heater-induced self absorption was low since the heater powers were low and was around 1–3 dB throughout the experiment. The selected ERPs were for the 9°S pointing direction since this heater wave was the one that passed through the UHF radar beam at the matching height. This was tested using the 3-D ray-tracing model of *Jones and Stephenson* [1975] to account for the refraction.

[35] In Figure 4, the two highest powers (52.3 and 104.5 MW) are clearly above the thresholds. This is consistent with Figure 3 where the signatures of both PDI and OTSI are apparent. For the 26.3 MW ERP pump pulses, the OTSI signature appears only for the two latter pulses and not the first. All three however show the enhanced shoulders associated with PDI. This is consistent with Figure 4 in that these pulses are indeed close to the modeled thresholds. For all of the lower pump powers where no PDI or OTSI signatures are detected, the modeling shows that the pump electric field is below the thresholds as observed.

[36] Figure 5 shows the CUTLASS radar backscatter from field-aligned density irregularities formed by the TPI in the heated region above EISCAT with a 3 s temporal resolution. The CUTLASS radar frequency band shown is for 16.5–16.7 MHz for beam 5 which looks over EISCAT. Backscatter occurs when the radar beam is perpendicular to the striations and the Bragg backscatter condition is met; i.e., the wave number of the striations is twice that of the radar. The radar was also recording at other frequencies in the vicinity of 10 and 13 MHz; however, no artificial backscatter was observed.

[37] The three cycles through the power steps can clearly be seen around range gate 32 with obvious backscatter occurring for the three highest pump powers (26.3, 52.3, and 104.5 MW ERP). There is also some backscatter from the fourth highest power (10.5 MW). The threshold for TPI, equation (8), where $k$ is twice the CUTLASS radar wave number calculated from the radar frequency, is shown in

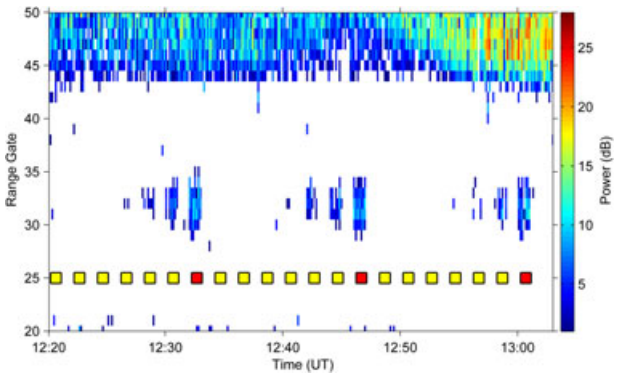


**Figure 5.** The CUTLASS radar backscatter from the heated region of the ionosphere during the experiment. The CUTLASS radar frequency was 16.5–16.7 MHz. The colored squares indicate when the pump was on, and the red squares show where the pump power was maximum.

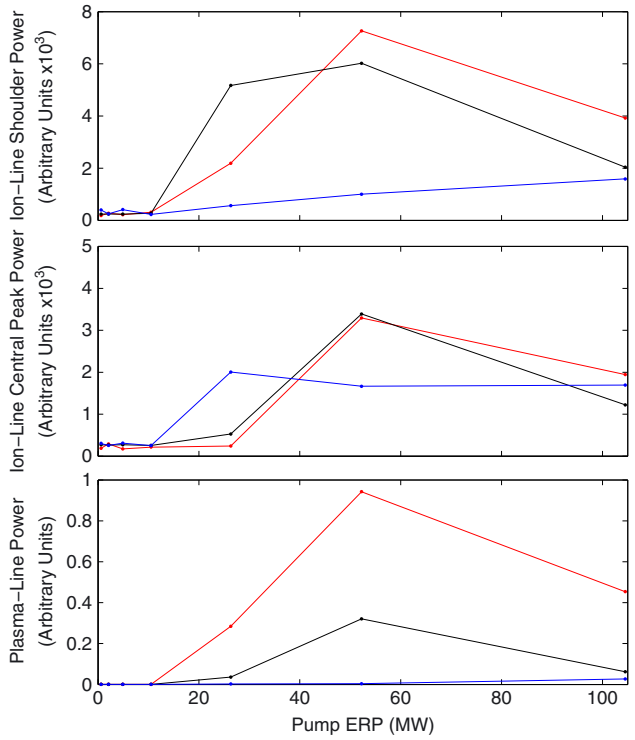


**Figure 6.** (top) The highest UHF ion line shoulder backscattered power for the first 5 s of pump on plotted against heater power. (middle and bottom) The same but for the ion line central peak and the plasma line, respectively. The colored lines separate the three pump power cycles. The red, black, and blue cycles were run first, second, and third, respectively.

Figure 4 in black. The model correctly predicts that the three highest powers (26.3, 52.3, and 104.5 MW ERP) exceed, or are close to, the TPI threshold. *Wright et al.* [2006] showed that low power pump waves (∼4–8 MW ERP) were able to generate striations, whereas we only see a clear signature of striations when pumping close to, or above, 26 MW ERP. We note that the pump frequency of the experiment performed by *Wright et al.* [2006] is lower at 4.544 MHz compared to the 7.953 MHz used here, and the frequency of the CUTLASS radar is lower too. Since the threshold for TPI depends on $k$ and $\omega_0^2$, we calculate that the threshold for striation generation in their experiment was ∼4 times lower than during ours. Therefore, the pump power in our experiment must be approximately 4 times as large before striations are observed: 26/4 = 6.5 MW, which is close to the 4 MW ERP estimated by *Wright et al.* [2006] to observe striations, ignoring $D$ region absorption differences. For 10.5 MW ERP and below, the modeling predicts the electric field is below the threshold for TPI, which is consistent with our observations of little to no CUTLASS backscatter.

[38] A possible explanation for the weakening of the backscattered power during the third pump cycle of the seven powers is that the orthogonality condition of the CUTLASS radar was no longer well satisfied; i.e., the striations were still as strong but the radar beam was less perpendicular to the magnetic field so not all of the scattered signal was being received. This can be due to a change in refraction of the radar beam as it travels to the region above EISCAT. When the radar beam is orientated in a less perpendicular manner, not all of the scattered signal will be received implying an apparent weakening of the striations [*Senior et al.*, 2004]. Altering the radar frequency slightly to counteract the change in refraction would correct this. It becomes difficult to determine therefore if the reduction in backscattered signal is because of the change in refraction or because the striations weaken.

[39] Another noticeable feature is the width of the backscattered region increases for increasing pump powers. This is because the ERP, and therefore the electric field strength, varies across the beam width, and there is a larger region in space where the ERP away from the center of the beam is large enough to stimulate TPI and therefore generate striations. For the lower powers, only the center of the beam has an ERP high enough to stimulate the TPI. The pump beam for the highest-power pump wave (104.5 MW ERP) has a half width of 9.6° where the ERP exceeds 26 MW and at 220 km in altitude corresponds to a full width of 80 km. The CUTLASS radar backscatter is observed over approximately 6–7 range gates, 15 km each, which is a region in space of the size 90–105 km. *Bryers et al.* [2012] found that the area of the pump wave due to refraction expanded by a factor of ∼1.2 compared to the free-space area. This would increase the area from 80 km to 96 km which lies within the measured range of 90–105 km. The modeled region is therefore in good agreement to the size of the true region in which TPI can develop.

[40] The top, middle, and bottom panels of Figure 6 show the UHF radar backscattered power for the highest ion line shoulder, the central peak, and the downshifted plasma line, respectively. The red, black, and blue lines show the first, second, and third ERP cycle, respectively. For the low pump powers, the backscattered power is low, whereas for the higher powers, it is increased. The most obvious feature is that the maximum backscattered power is found for the second highest pump power (52.3 MW ERP) and for the highest pump power, the backscattered signal is reduced again. This may be because the pump wave is anomalously absorbed by the striations, so that the power which is available to drive the PDI and OTSI diminishes and consequently, the ion acoustic waves weaken. For lower-amplitude striations, the anomalous absorption is not as great and strong ion acoustic and Langmuir waves are still produced [*Robinson*, 1989]. Increasing temperatures as the heater power increases (see Figure 1) could also be responsible for this weakening at the highest power. As the electron temperature increases, the Langmuir wave is damped more via Landau damping [*Westman et al.*, 1995], yet conversely, the ion acoustic wave is dampened less. This implies that the plasma instabilities are affected by Landau damping; however, the overall effect on the enhanced ion and plasma line power is unclear due to the two opposing effects the enhanced temperatures have.

[41] It is well known that the striations cause anomalous absorption giving rise to the ion line overshoot effect. This is where the enhanced ion line is strongly enhanced in the first few seconds of pump on and then diminishes in power on timescales associated with the striation growth of a few seconds [*Jones et al.*, 1986]. Figure 7 shows the UHF radar backscattered signal during the experiment for the highest ion line shoulder (top), the ion line central peak (middle),

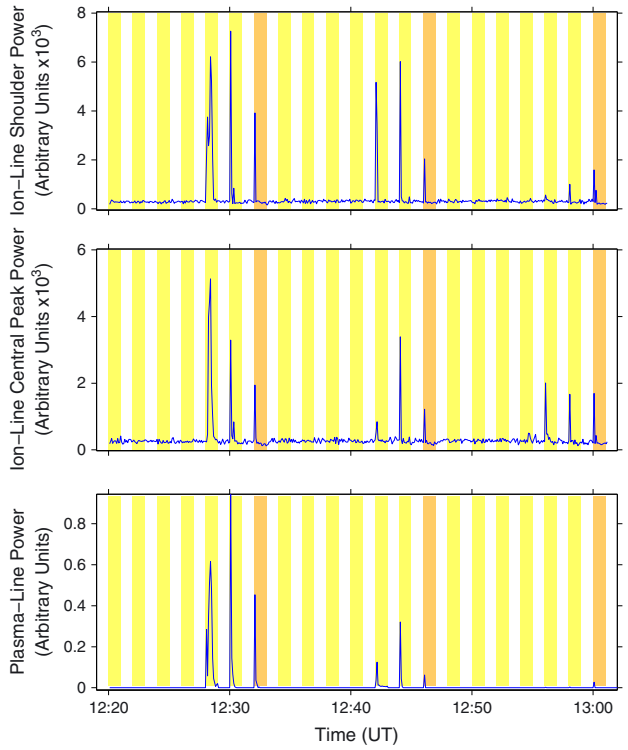


**Figure 7.** (top) The highest UHF ion line shoulder backscattered power during the experiment. (middle and bottom) The same but for the ion line central peak and the plasma line, respectively. The yellow areas show when the pump was on, and the orange section shows when the pump power was at its maximum (104.5 MW ERP).

and the downshifted plasma line (bottom). The yellow areas show when the pump was on, and the orange section shows when the pump power was at its maximum (104.5 MW ERP). For the third highest power (26.3 MW ERP), the ion line enhancement is generally more persistent than for the two higher powers and continues to grow in strength during pump on. For the 52.3 and 104.5 MW ERP pump powers, the ion line enhancement is only present in the first 5–10 s of pump on typically, i.e., the ion line overshoot effect. For the second and third experiment cycle, the enhancement is not as persistent for the 26.3 MW ERP pump pulse which may be because of ionospheric preconditioning.

[42] *Wright et al.* [2006] showed that the backscattered power from the CUTLASS radar was greater when the ionosphere had been preconditioned. They ran an experiment whereby they increased the heater power from 0 to 155 MW in approximately 4 MW steps and then slowly decreased it again. The backscattered power from the CUTLASS radar exhibited hysteresis and was higher for the same pump powers on the downward leg of the power stepping. *Wright et al.* [2006] also showed that a short high-power "seed pulse" before longer low-power pumping produced a higher backscatter than is observed for pumping with no seed pulse. These two effects are a form of preconditioning and occur because a power threshold has to be exceeded for striations to grow, but once they exist, a lower power can maintain them as long as it is above a second, lower threshold. Figures 6 and 7 show that the UHF radar enhancements toward the end of the experiment are not as great as those at the start. This observation can be explained by preconditioning so the striations become more easily excited, and therefore, anomalous absorption of the pump wave is higher and the UHF backscatter enhancements weaken.

[43] Figure 8 introduces data taken from the SEE recording equipment and shows the SEE power plotted at the DM frequency peak of 7.942 MHz, so $\Delta f_{DM}$ = 11 kHz. This is slightly less than the frequency offset predicted by $\Delta f_{DM} = 2 \times 10^{-3} f_0$ = 15.9 kHz, [*Stubbe et al.*, 1984] for $f_0$ = 7.953 MHz which could be due to the difficulty in determining the peak since it it is observed to have a wide plateau. During this experiment, the LH frequency is $\omega_{lh} \sim$ 7.8 kHz and $\Delta f \sim$ 8 kHz which is the offset of the highest DM frequency from $f_0$ (not the peak, $\Delta f_{DM}$). This result is in agreement with other observations [*Leyser et al.*, 1990]. The power of the DM peak is increasing with pump power and appears to be present for all but the lowest pump power where the signal becomes comparable in strength to the background noise. It is difficult to distinguish this increase in power at the DM frequency for the low pump powers from the background continuum power which also increases during pump on for all powers. The background continuum increase is pump power dependent, so the contribution of this increase in power at 7.942 MHz is difficult to attribute to the DM mechanism alone. For this reason the plot in Figure 8 shows the power at $f_0$ – 6 kHz subtracted from the power at the DM frequency. This is an attempt to remove the contamination from the continuum; however, it is not perfect. Inspection of the individual SEE spectra suggests that the DM only exists for three highest pump powers (26.3, 52.3, 104.5 MW), below which, no obvious increase above the gradual gradient of the continuum is noticeable, which agrees with Figure 8.

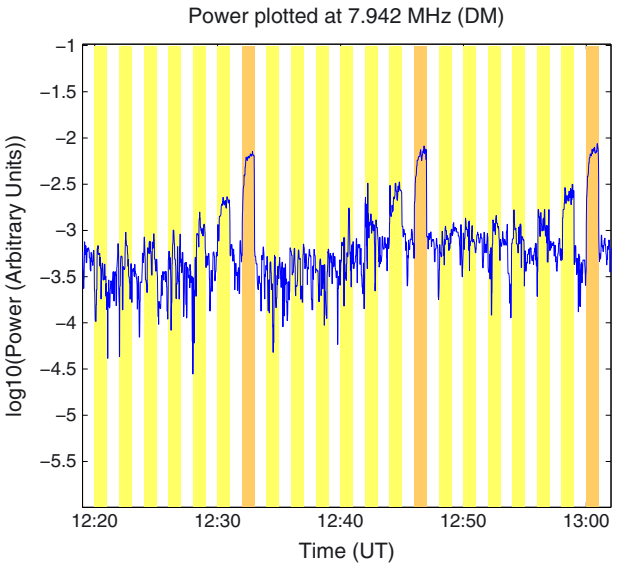


**Figure 8.** SEE data plotted at the downshifted maximum frequency of 7.942 MHz (11 kHz below the pump frequency). The yellow areas show when the pump was on, and the orange section shows when the pump power was at its maximum (104.5 MW ERP).

[44] The presence of the DM indicates the presence of striations and UH waves. Figure 5 shows only striations at one wave number determined by the CUTLASS radar wave number. If multiple radar frequencies were incident upon the heated volume of the ionosphere, we would perhaps observe striations for lower powers too since the TPI mechanism by which the striations develop, with a threshold given by equation (8), is dependent upon the wave number, $k$ of the striations being observed. Since the CUTLASS radar can only observe certain striation wave numbers limited by the Bragg condition, we conclude that the SEE is a much more sensitive tool for observing the presence of striations since it does not discriminate against striation wave numbers. The fact that we mainly see striation signatures only for the three highest powers by both diagnostics seems to suggest that there is a minimum striation wave number that can exist. Striations with a smaller wave number must not be generated by the pump wave of this frequency since otherwise it would be observable in the SEE data.

[45] Another feature of interest in Figure 8 is that for the highest pump power especially where the SEE signal-to-noise ratio at the DM is higher, the growth time of the DM can be seen and appears to reach a maximum after approximately 40 s.

## 5. Summary and Conclusions

[46] We have demonstrated that the theoretical thresholds of three plasma wave instabilities are consistent with modeling of an ionospheric plasma pumping experiment. The theory regarding electric field thresholds of PDI, OTSI, and TPI was compared with an electric field model of the pump wave taking $D$ region absorption into account. The modeled electric fields of the pump wave and the thresholds agree with observations made using the UHF radar for detecting plasma waves generated by the PDI and OTSI and the CUTLASS radar for observing striations associated with the TPI. We conclude that the PDI and OTSI electric field thresholds are approximately 0.25 and 0.3 V/m, respectively and the TPI threshold is $\sim$0.3 V/m. During the experiment, the ionospheric conditions meant that pumping with an ERP of $\sim$26 MW was needed to generate striations and overcome the $D$ region absorption. On other days, the $D$ region absorption could vary significantly so a different ERP threshold would be observed.

[47] At higher ERPs (>52.3 MW), we observe the effect striations have on the anomalous self-absorption of the pump wave as it couples to, and drives ion acoustic, Langmuir and upper hybrid waves in the plasma close to the HF reflection altitude. The striations act to diminish the pump wave power to a level below that required to drive the PDI and OTSI. For high pump powers, where striations are deeper, only an ion line overshoot effect is observed; i.e., the enhancement in the UHF spectra is short lived for a few seconds. For lower pump powers, the striations have a smaller effect on the self-absorption and the enhancements can persist, sometimes for the entire duration of the pump pulse.

[48] **Acknowledgments.** EISCAT is an international scientific association supported by research organizations in China (CRIRP), Finland (SA), Japan (NIPR and STEL), Norway (NFR), Sweden (VR), and the United Kingdom (NERC).

[49] Robert Lysak thanks the reviewers for their assistance in evaluating this paper.

## References

Ashrafi, M., M. Kosch, and F. Honary (2006), Heater-induced altitude descent of the EISCAT UHF ion line enhancements: Observations and modeling, *Adv. Space Res.*, *38*, 2645–2652.

Baron, M. (1984), The EISCAT facility, *J. Atmos. Terr. Phys.*, *46*, 469–472.

Brändström, B. U. E., T. B. Leyser, A. Steen, M. T. Rietveld, B. Gustavsson, T. Aso, and M. Ejiri (1999), Unambiguous evidence of HF pump-enhanced airglow, *Geophys. Res. Lett.*, *26*, 3561–3564.

Bryers, C. J., M. J. Kosch, A. Senior, M. T. Rietveld, and T. K. Yeoman (2012), EISCAT observations of pump-enhanced plasma temperature and optical emission excitation rate as a function of power flux, *J. Geophys. Res.*, *117*, A09301, doi:10.1029/2012JA017897.

Bond, G. E., T. R. Robinson, P. Eglitis, D. M. Wright, A. J. Stocker, M. T. Rietveld, and T. B. Jones (1997), Spatial observations by the CUTLASS coherent scatter radar of ionospheric modification by high power radio waves, *Ann. Geophys.*, *15*, 1412–1421, doi:10.1007/s00585-997-1412-4.

Budden, K. G. (1961), *Radio Waves in the Ionosphere*, Cambridge Univ. Press, London and New York.

Chisham, G., et al. (2007), A decade of the Super Dual Auroral Radar Network (SuperDARN): Scientific achievements, new techniques and future directions, *Survey. Geophys.*, *28*, 33–109.

Das, A., and J. Fejer (1979), Resonance instability of small-scale field-aligned irregularities, *J. Geophys. Res.*, *84*, 6701–6704, doi:10.1029/JA084iA11p06701.

Evans, J. V. (1969), Theory and practice of ionosphere study by Thomson scatter radar, *Proc. IEEE*, *57*, 496–530.

Fejer, J. A. (1979), Ionospheric modification and parametric instabilities, *Rev. Geophys.*, *17*, 135–153, doi:10.1029/RG017i001p00135.

Fialer, P. A. (1974), Field-aligned scattering from a heated region of the ionosphere observations at HF and VHF, *Radio Sci.*, *9*, 923–940.

Frolov, V. L. (1991), Some remarks on the dynamics of artificial ionospheric radio emission, paper presented at the IIIrd Suzdal URSI Symposium on Modification of the Ionosphere by Powerful Radio Waves (ISIM-3), Union Radio Sci. Int., Moscow, Russia.

Grach, S. M., and V. Y. Trakhtengerts (1975), Parametric excitation of ionospheric irregularities extended along the magnetic field, *Radiophys. Quant. Electron.*, *18*, 951–957.

Greenwald, R. A., et al. (1995), DARN/SUPERDARN: A global view of the dynamics of high-latitude convection, *Space. Sci. Rev.*, *71*, 761–796.

Gustavsson, B., M. T. Rietveld, N. V. Ivchenko, and M. J. Kosch (2010), Rise and fall of electron temperatures: Ohmic heating of ionospheric electrons from underdense HF radio wave pumping, *J. Geophys. Res.*, *115*, A12332, doi:10.1029/2010JA015873.

Honary, F., T. R. Robinson, D. M. Wright, A. J. Stocker, M. T. Rietveld, and I. McCrea (1999), Letter to the Editor: First direct observations of the reduced striations at pump frequencies close to the electron gyroharmonics, *Ann. Geophys.*, *17*, 1235–1238.

Jones, R. M., and J. J. Stephenson (1975), A versatile three-dimensional ray tracing computer program, Office of Telecommunications Report 75-76, US Government Printing Office, Washington, D. C., 20402, USA.

Jones, T. B., T. R. Robinson, P. Stubbe, and H. Kopka (1986), EISCAT observations of the heated ionosphere, *J. Atmos. Terr. Phys.*, *48*, 1027–1035.

Leyser, T. B., B. Thidé, H. Derblom, Å. Hedberg, B. Lundborg, P. Stubbe, and M. T. Rietveld (1989), Stimulated electromagnetic emission near electron cyclotron harmonics in the ionosphere, *Phys. Rev. Lett.*, *63*, 1145–1147.

Leyser, T. B., B. Thidé, H. Derblom, Å. Hedberg, B. Lundborg, P. Stubbe, and H. Kopka (1990), Dependence of stimulated electromagnetic emission on the ionosphere and pump wave, *J. Geophys. Res.*, *95*, 17,233–17,244.

Leyser, T. B., B. Thidé, M. Waldenvik, E. Veszelei, V. L. Frolov, S. M. Grach, and G. P. Komrakov (1994), Downshifted maximum features in stimulated electromagnetic emission spectra, *J. Geophys. Res.*, *99*, 19,555–19,568, doi:10.1029/94JA01399.

Leyser, T. B. (2001), Stimulated electromagnetic emissions by high-frequency electromagnetic pumping of the ionospheric plasma, *Space Sci. Rev.*, *98*, 223–328.

Löfas, H., N. Ivchenko, B. Gustavsson, T. B. Leyser, and M. T. Rietveld (2009), F-region electron heating by X-mode radiowaves in underdense conditions, *Ann. Geophys.*, *27*, 2585–2592.

Rietveld, M. T., H. Kohl, H. Kopka, and P. Stubbe (1993), Introduction to ionospheric heating at Troms. Part I: Experimental overview, *J. Atmos. Sol. Terr. Phys.*, *55*, 577–599.

Robinson, T. R. (1989), The heating of the high latitude ionosphere by high power radio waves, *Phys. Rep.*, *179*, 79–209.

Senior, A., N. D. Borisov, M. J. Kosch, T. K. Yeoman, F. Honary, and M. T. Rietveld (2004), Multi-frequency HF radar measurements of artificial F-region field-aligned irregularities, *Ann. Geophys.*, *22*, 3503–3511.

Senior, A., M. T. Rietveld, M. J. Kosch, and W. Singer (2010), Diagnosing radio plasma heating in the polar summer mesosphere using cross-modulation: Theory and observations, *J. Geophys. Res.*, *115*, A09318, doi:10.1029/2010JA015379.

Shoucri, M. M., and G. J. Morales (1984), Ohmic heating of the polar F-region by HF pulses, *J. Geophys. Res.*, *89*, 2907–2917.

Shvarts, M. M., and S. M. Grach (1997), Interaction of upper and lower hybrid waves and generation of the downshifted maximum feature of stimulated electromagnetic emissions, *J. Atmos. Terr. Phys.*, *59*, 2421–2429.

Stubbe, P. H., and H. Kopka (1981), *Exploration of the Polar Upper Atmosphere: Proceedings of the Nato Advanced Study Institute,* edited by C. S. Deehr and J. A. Holtet, D. Reidel Pub. Co., The Netherlands, doi:10.1007/978-94-009-8417-2_6.

Stubbe, P., H. Kopka, T. B. Jones, and T. Robinson (1982), Wide band attenuation of radio waves caused by powerful HF waves: Saturation and dependence on ionospheric variability, *J. Geophys. Res.*, *87*, 1551–1555, doi:10.1029/JA087iA03p01551.

Stubbe, P., and H. Kopka (1983), Summary of results obtained with the Tromso heating facility, *Radio Sci.*, *18*, 831–834, doi:10.1029/RS018i006p00831.

Stubbe, P., H. Kopka, B. Thidé, and H. Derblom (1984), Stimulated electromagnetic emission: A new technique to study the parametric decay instability in the ionosphere, *J. Geophys. Res.*, *89*, 7523–7536, doi:10.1029/JA089iA09p07523.

Stubbe, P., H. Kohl, and M. T. Rietveld (1992), Langmuir turbulence and ionospheric modification, *J. Geophys. Res.*, *97*, 6285–6297.

Thidé, B., H. Kopka, and P. Stubbe (1982), Observations of stimulated scattering of a strong high-frequency radio wave in the ionosphere, *Phys. Rev. Lett.*, *49*, 1561–1564.

Thomson, J. A. (1970), Energy deposition in artificial ionospheric heating experiments, *J. Geophys. Res.*, *75*, 6446–6452, doi:10.1029/JA075i031p06446.

Vaskov, V. V., and A. V. Gurevich (1975), Nonlinear resonant instability of a plasma in the field of an ordinary electromagnetic wave, *J. Sov. Phys. JETP, Eng. Transl.*, *42*, 91–97.

Westman, A., T. B. Leyser, G. Wannberg, and M. T. Rietveld (1995), Tristatic EISCAT-UHF measurements of the HF modified ionosphere for low background electron temperatures, *J. Geophys. Res.*, *100*, 9717–9728, doi:10.1029/94JA03337.

Wright, D. M., J. A. Davies, T. K. Yeoman, T. R. Robinson, and H. Shergill (2006), Saturation and hysteresis effects in ionospheric modification experiments observed by the CUTLASS and EISCAT radars, *Ann. Geophys.*, *24*, 543–553, doi:10.5194/angeo-24-543-2006.